A Vapor−Solid Strategy to Silica Sheathed Metal Nanostructures and Microstructures via Reactions of Metal Chlorides with Silicon

Jin Wang,[†] Haoxu Zhang,[‡] Jianping Ge,[†] and Yadong Li*[,†]

Department of Chemistry, Tsinghua University, Beijing 100084, People's Republic of China, and Nanoscale Physics & Devices Laboratory, Institute of Physics, Chinese Academy of Science, Beijing 100080, People's Republic of China

Received: September 12, 2005; In Final Form: November 4, 2005

A facile vapor−solid strategy has been developed to prepare silica-sheathed metal micro/nanostructures with controllable shapes. As examples, silica-sheathed nickel nanowires (diameter ∼50 nm), microcubes (edge length 1−3 μm), nanocubes (edge length ∼200 nm) with an epitaxial tail (diameter <100 nm), and 1D assembly structures of nanoparticles (particle diameter <100 nm) as well as silica-sheathed cobalt and copper micro/nanostructures are synthesized. The possible reaction and growth mechanisms of Ni/SiO_2 structures are discussed. The method is expected to be applied to a wider range of metals.

1. Introduction

In recent years, because small size could enrich materials with versatile chemical and physical properties of novelty, micro/nanostructures have become one of the most active fields both in science research and practical applications. Various fabrication approaches have been developed and have provided more multiple and complex units and systems for investigations.[1−11] Chemical vapor deposition (CVD), which had been widely used in preparing films, was introduced into this area and proved to be a very effective method, characterized by many advantages such as facility and adjustability.[12−15] In particular, atmospheric pressure chemical deposition (APCVD) is the simplest type of CVD, which allows for high throughput and continuous operation at low cost. We have successfully prepared a series of sulfide and silicate nanostructures with it and demonstrated that the chlorides are ideal candidate precursors in the APCVD methods due to their relatively high vapor pressure and adequate reactivity.[16−19]

During the research process of exploring the application of chloride-precursor APCVD, we found an interesting phenomenon by chance that vapor $NiCl_2$ could react with a Si wafer and produce a dominant phase of metal Ni with the characteristic dimension of less than a micrometer and small amounts of Ni silicides. Ni nanoparticles are known as a catalyst in the VLS growth of many 1D nanostructures as well as in industrial manufacture, and their magnetic properties endow them with rich theoretical and practical meanings;[20] nickel silicides are also very important electronic materials.[21] So it is attractive for us to obtain small particles of pure Ni or its pure phase silicide through investigation of the phenomenon. Luckily, after a series of experiments, we succeeded to synthesize diversified micro/nanostructures of pure Ni and found the new method we used was rather general.

The nickel particles with well-controlled shapes from nanowires, microcubes, and nanocubes with an epitaxial tail to 1D assembly structures of nanoparticles were obtained. They were coated with amorphous silica during the synthesis process. Furthermore, the method was extended to cobalt and copper and proven to be an effective approach to shape-controlled synthesis of metals. To clearly describe experimental results, we denote the as-prepared particles with different experimental parameters (Table 1) as Sample 1, Sample 2 and so on.

2. Experimental Section

The experiments were conducted in a furnace with a horizontal quartz tube of 2.70 cm in the inner diameter and 110 cm in length. The metal chloride powders, which had been dehydrated via heating in a vacuum of tens of Pa (specifically, $NiCl_2 \cdot 6H_2O$ and $CoCl_2 \cdot 6H_2O$ were heated at 220 °C for 15 min and $CuCl_2 \cdot 2H_2O$ was heated at 150 °C for 15 min), was put in an alumina boat in the middle of the furnace. Another alumina boat containing silicon powders and a (110) alumina substrate was placed downstream away from the metal chloride. A smaller quartz tube with one end open toward the downstream direction (length, 20 cm; outer diameter, 2.05 cm; inner diameter, 1.90 cm) was selectively used as an accessory to hold the alumina boats according to Table 1. The apparatus was evacuated and filled with pure nitrogen. Then a nitrogen flow of 25 cm^3(STP) min^{-1} was used as the carrier gas. The temperature of the furnace was raised to the designated temperature from room temperature at a rate of 10 °C/min and maintained for 60 min. Then the furnace was cooled to room temperature naturally. The location of the silicon powders and the alumina substrate, the furnace center temperature and the amount of the used metal chloride varied as listed in Table 1. Scheme 1 illustrates the apparatus setting for the preparation of Sample 1 as an example. It should be mentioned that a (100) silicon wafer is used to replace silicon powders and the alumina substrate in the experiment for Sample 4, and its reproduction is harder than the others.

The synthesized products were characterized by scanning electron microscopy (SEM, Sirion 200), energy-dispersive analysis (EDS, Sirion 200), X-ray diffraction (XRD, Brüker D8 Advance X-ray diffractometer), transmission electron micro-

* To whom correspondence should be addressed. E-mail: ydli@tsinghua.edu.cn; Tel: 86-10-62772350, Fax: 86-10-62788765.
[†] Tsinghua University.
[‡] Chinese Academy of Science.

10.1021/jp055139g CCC: $33.50
Published on Web 12/21/2005

TABLE 1: Experimental Parameters of the Discussed Samples

sample number	starting materials	furnace center temperature	Si powder location	Al_2O_3 substrate location	existence of smaller quartz tube
1	0.050 g $NiCl_2$ 0.016 g Si	700 °C	1.75 cm	1.50 cm	Yes
2	0.050 g $NiCl_2$ 0.016 g Si	900 °C	6.00 cm	6.25 cm	Yes
3	0.050 g $NiCl_2$ 0.016 g Si	650 °C	1.75 cm	1.50 cm	Yes
4	0.100 g $NiCl_2$ (silicon wafer)	900 °C	11.50 cm (silicon wafer)	11.50 cm (silicon wafer)	No
5	0.050 g $NiCl_2$ 0.016 g Si	900 °C	6.00 cm	6.25 cm	No
6	0.050 g $NiCl_2$ 0.016 g Si	900 °C	10.25 cm	10.50 cm	Yes
7	0.050 g $CoCl_2$ 0.016 g Si	700 °C	1.75 cm	1.50 cm	Yes
8	0.050 g $CoCl_2$ 0.016 g Si	850 °C	5.50 cm	5.75 cm	Yes
9	0.050 g $CuCl_2$ 0.016 g Si	700 °C	1.75 cm	1.50 cm	Yes
10	0.050 g $CuCl_2$ 0.016 g Si	800 °C	5.50 cm	5.75 cm	Yes

SCHEME 1: Apparatus Scheme for the Preparation of Sample 1 as an Example

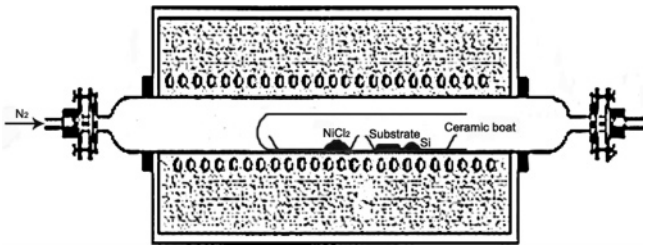

scopy (TEM, JEM-1200EX), and high-resolution transmission electron microscopy (HRTEM, Tecnai G2 F20 S-Twin).

3. Results and Discussion

3.1 Different Morphologies of Ni/SiO_2 Structures. Figure 1a presents a typical scanning electron microscopy (SEM) image of Sample 1. The Al_2O_3 substrate was covered with curly nanowires up to tens of micrometers long, which can be identified as pure face-centered cubic (fcc) nickel with a lattice constant of $a = 0.3523$ nm (JCPDS, No.04-0850) by the XRD result (Figure 1b). TEM results reveal that the as-prepared nanowires have core−shell structure with typical outer diameter of 200 nm and core diameter of 50 nm, as the example shown in Figure 1c. Figure 1d shows the tail part of a long nanowire. As the nanowire goes to the end, the core becomes thinner and thinner while the outer diameter remains unchanged. The selected area electron diffraction (SAED) pattern recorded from the marked region can be indexed to the same fcc phase as has been designated by the XRD result. Meanwhile, the SAED pattern from only the shell part does not show the feature of crystals. So it is safe to conclude that the core is a nickel phase and the shell is noncrystalline. Additionally, the (220) direction of the SAED pattern is roughly parallel to the axis of the marked core part, which suggests that the nickel wire should grow along the (220) direction in good accord with the previous literature.[22] Further investigation with the energy-dispersive spectrum (EDS, Figure 1e, obtained by analyzing the attached part on the conductive tape from Sample 1) indicates that the nanowires consist of Ni, O, and Si, and the ratio of Si to O is approximately 1:2. Combined with the previous SAED analysis, the shell can be determined to be noncrystalline SiO_2.

Figure 2a and its inset are the SEM and TEM images of Sample 2, respectively. Well-defined cubes with edge length ranging from 1 to 3 μm were deposited on the (110) Al_2O_3 substrate. No obvious silica sheath could be seen from the TEM image, but the EDS result (Figure S1 in the Supporting Information, obtained by analyzing one of the detached cubes on the conductive tape from Sample 2) shows the existence of a small amount of SiO_2, in addition to Ni, which indicates that a very thin layer of silica surrounds the nickel core.

XRD pattern (Figure 2b) definitely confirms these cubes are fcc nickel crystals (JCPDS, No.04-0850). Something worthy of note is that the Ni (2 0 0) peak greatly overwhelms the other

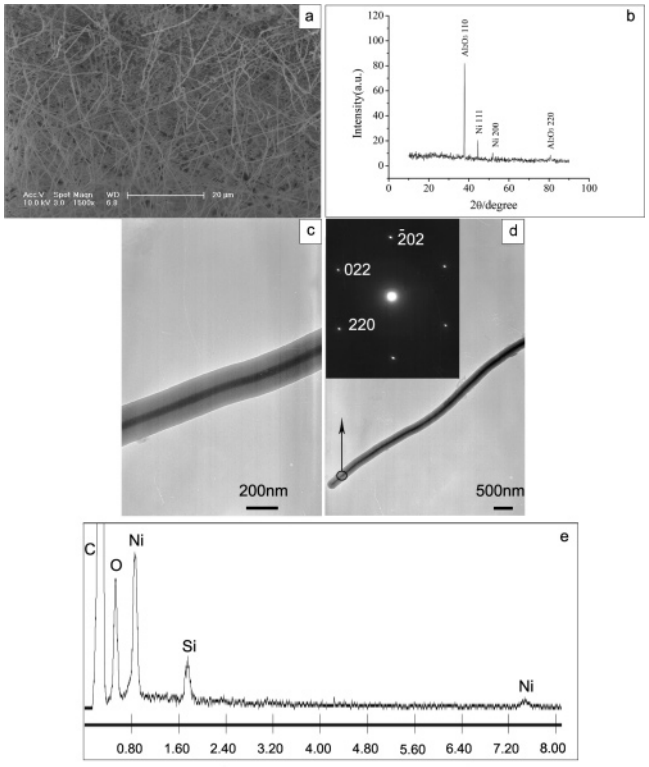

Figure 1. (a) Typical SEM image of Sample 1. (b) XRD pattern for Sample 1. (c) Typical TEM image of Sample 1. (d) TEM image of the tail part of a long silica-sheathed nickel wire (inset: the SAED pattern recorded from the marked region). (e) EDS spectrum of Sample 1.

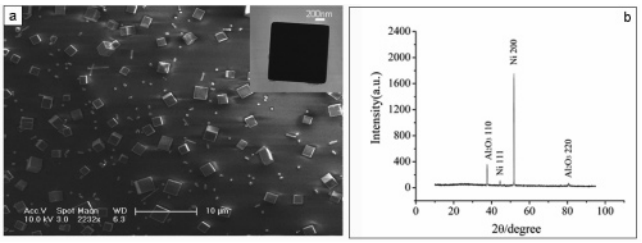

Figure 2. (a) SEM image of Sample 2 (inset: TEM image of a single microcube). (b) XRD pattern for Sample 2.

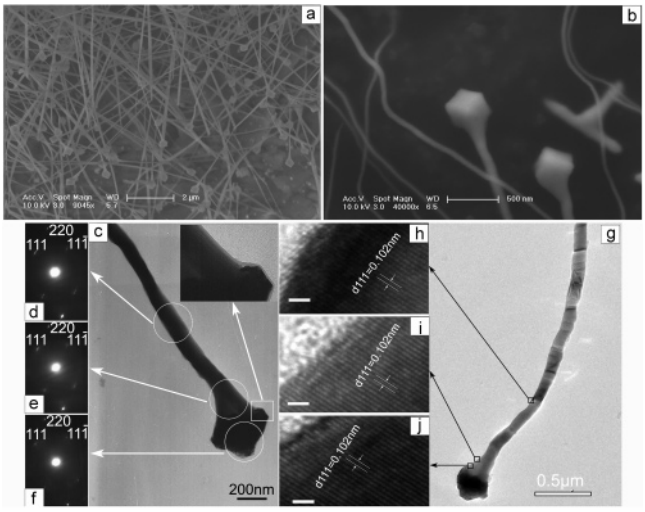

Figure 3. (a) SEM image of Sample 3. (b) Higher magnificaiton SEM image of Sample 3. (c) TEM image of Sample 3 (inset: magnified image of the marked rectangular region). (d, e, f) SAED patterns of the marked circle regions of Figure 3c. (g) TEM image of Sample 3. (h, i, j) HRTEM images of the marked rectangular regions of Figure 3g, scale bar 1 nm.

ones while in powder diffraction pattern the Ni (200) peak is only about 50% of the strongest (111) peak in intensity. It can be explained as follows. The well-defined cubic morphology is characteristic of single-crystalline cubic-structured Ni crystals bound by six {1 0 0} planes. Meanwhile, as shown by the SEM image, almost every microcube is located with two of the six outer facets parallel to the Al_2O_3 substrate (110) surface to keep stable. Therefore, the reflection of crystal planes corresponding to these six equivalent facets should give rise to the dominant (200) peak detected by XRD.

SEM images in Figure 3a and 3b portray the morphology of Sample 3. The typical unit is a nanocube with a long tail, up to several microns, which turns thinner and thinner as growing farther from the nanocube. The edge length of the nanocubes is estimated to be 200 nm and the diameter of the tails is less than 100 nm. The inset of Figure 3c shows that both the nanocubes and their tails have a sheath. The SAED patterns (Figure 3d, 3e and 3f) of the cube part, the neck part and the tail part can be indexed into the same nickel fcc structure and have a uniform orientation. As shown in Figure 3d, the (111) direction is roughly parallel to the tail axis, indicating that the tail grows along (111) direction. Meanwhile, the consistence of the SAED patterns of the tail part, the neck part, and the cube part demonstrates that the growth of the tail is an epitaxial process with the (111) crystal plane of the cube as the epitaxial plane. Figure 3h, 3i, and 3j are HRTEM images of the marked regions of another cube-tail structure, clearly elucidating the uniformly oriented (111) growth plane along the whole tail.

Assemblies of nickel nanoparticles/nanorods embedded in silica 1D nanostructures were found in Sample 4, as shown in

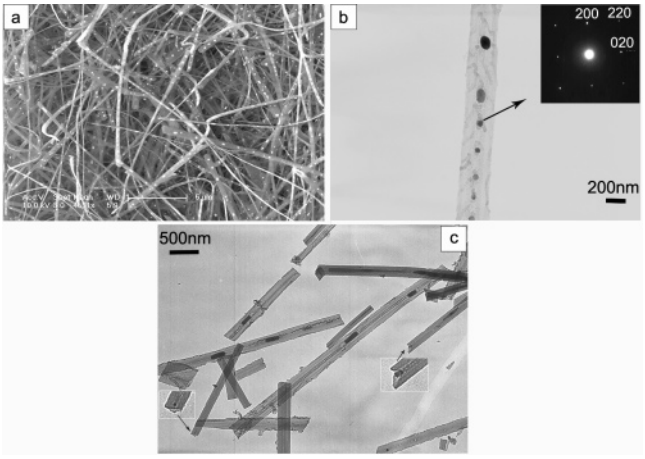

Figure 4. (a) SEM image of Sample 4. (b) TEM image of 1D assembly of nanoparticles in a nanobelt. (c) TEM image of 1D assembly of nanoparticles or nanorods in nanotubes.

Figure 4a. The silica 1D nanostructures mainly have two types: nanobelts and nanotubes. The former can be easily found in both the SEM image (Figure 4a) and the TEM image (Figure 4b), with width ranging from 300 to 500 nm and thickness of about 20 nm. The latter could be clearly seen in the TEM image (Figure 4c) with an obvious characteristic of open ends shown by the magnified part. The assemblies of several short nanorods are also observed. The SAED pattern (the inset of Figure 4b) recorded from the marked nanoparticle confirms the nanoparticles are nickel. The EDS result from a large area of the as-prepared 1D assembly structures demonstrates the products contain only Ni, Si, and O. The quantitive analysis tells us the ratio of Si to O is 1:2, while the corresponding value of Si to Ni is 7:1, which indicates that such assemblies in which nickel nanoparticles are sparely embedded in the silica matrix occur only when the amount of formed SiO_2 is much larger than that of formed Ni.

3.2 Reaction and Growth Mechanism. The above section has exhibited various micro/nanostructures assembled with nickel and silica, but a basic question of how the two kinds of assembly units came out from the source materials $NiCl_2$ and Si is still unsolved. As shown in the Experimental Section, $NiCl_2$ and Si were placed in different ceramic boats and thus a transfer process was needed for them to contact with each other. Over our experimental temperature range, $NiCl_2$ could be easily vaporized giving the partial pressure of a few millibar at 650 °C while almost no Si vapor could be produced from the silicon powders. When $NiCl_2$ gas contacted with the Si powders, the possible reaction occurred as follows:

$$2NiCl_2 + Si \rightarrow 2Ni + SiCl_4 \quad (1)$$

The produced fresh Ni species existed in the vapor phase and rapidly deposited on the Al_2O_3 substrate, the top of the Si powders, and the nearby ceramic boat wall. At the same time, the simultaneously formed $SiCl_4$ readily reacted with O_2 or H_2O gas, which had leaked into the quartz tube or desorbed from the tube wall at a high temperature (trace amount of water in the dehydrated chlorides may also serve as a source), giving products as shown by the equations below:

$$SiCl_4 + O_2 \rightarrow SiO_2 + 2Cl_2 \quad (2)$$

$$SiCl_4 + 2H_2O \rightarrow SiO_2 + 4HCl \quad (3)$$

The nearly simultaneously formed SiO_2 relative to Ni tended

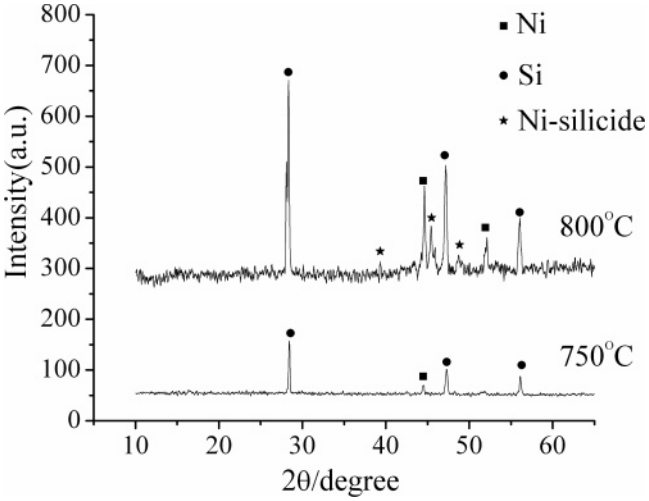

Figure 5. XRD patterns for remained silicon powders at different reaction temperatures.

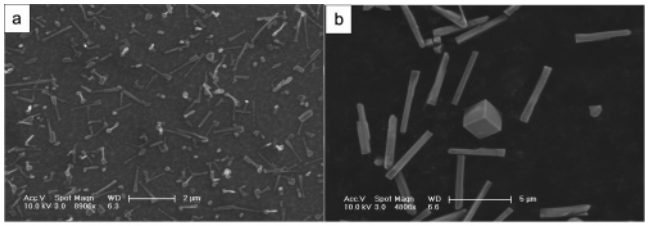

Figure 6. (a) SEM image of Sample 5. (b) SEM image of Sample 6.

to adsorb onto the Ni surface and form a sheath around the Ni particles. Reactions 2 and 3 have been comprehensively investigated,[23] and it has been pointed that the SiO_2 obtained via them is always amorphous and nanoscaled. This is consistent with our experiments.

The chemical stability of the deposited Ni and SiO_2 is also confirmed by the previous research.[24] Lee et al. calculated the ternary phase diagram of Ni−Si−O and found that a tie line exists between Ni and SiO_2, indicating that the two phases will coexist without any reaction. Experimentally, they found that the reactivity of Ni and SiO_2 depends strongly on the silicon oxide nature. The native SiO_2 layer formed with incorporation of water or moisture is stable in contact with pure Ni while the thermal SiO_2 grown by dry oxidation will react with Ni to form NiO. The growth environment of our products in the presence of water determined that the final deposits of Ni and SiO_2 are stable.

In addition, we analyzed the Si powders with XRD after the experiment and detected nickel silicides in addition to nickel and excess silicon in some experiments, such as those for preparing Sample 2 and Sample 4. Correlating the appearance of nickel silicide with the temperature of Si powders during the temperature maintaining period of the furnace, we found that no nickel silicides appeared from 650 °C to 750 °C while obvious silicides could be detected above 800 °C (Figure 5). Taking in consideration that the deposits on the Al_2O_3 substrate had no silicides but pure nickel in any experiment listed in Table 1, we conjectured that the silicides came from the reaction of Ni and unreacted Si. Lee et al. reported that Ni films did not react with the silicon wafer with a native silica layer until 800 °C.[24] This is in good accord with our experiment facts and sufficiently confirmed the origin of the nickel silicides.

There are mainly two mechanisms to explain the growth of 1D structure in the vapor phase: vapor−liquid−solid (VLS) mechanism and vapor−solid (VS) mechanism. The characteristic feature of VLS mechanism is the existence of a catalyst nanoparticle at the tip of the nanowire. The absence of such nanospheres indicates the VS mechanism should be responsible for the growth of the silica-sheathed nickel nanowires. After the reaction of $NiCl_2$ and Si, Ni species were produced and nucleated on the substrate surface when the concentration reached a certain supersaturation. Then newly generated nickel species were absorbed on the nuclear surface, and meanwhile some outer nickel atoms of the nucleus were vaporized. The two competitive processes made only the nickel atoms packing on the growth crystal plane stable in the solid phase, and thus led to the 1D prolongation of the crystal. At the same time, the almost simultaneously formed SiO_2 adhered to the surface of the nickel nanowire as a sheath. Recently Zhang et al. synthesized silica-sheathed Fe_7S_8 nanowires via a CVD method and proposed that SiO_2 were preferentially absorbed on some certain Fe_7S_8 surfaces and induced the 1D growth of Fe_7S_8.[25] Perhaps some similar roles of SiO_2 in our method may be taken into consideration.

Microcubes are also dominated by VS mechanism under the condition of much higher supersaturation of deposited product species. To achieve this, in addition to the relatively high temperature, we inserted a thinner quartz tube with one closed end into the outer quartz tube to hold the ceramic boat of $NiCl_2$ and another one of Si powders and the substrate. Such an accessory could restrict the gas-phase species to diffuse in a smaller volume of space and thus keep higher concentrations. The product (Sample 5) obtained from the experiment with the same parameters as Sample 2 except for the absence of the inserted thinner quartz tube are shown in the Figure 6a, in the shape of nanorods rather than microcubes due to the lower concentration of deposited species. With varying the location of Si powders and the Al_2O_3 substrate from 6.00 to 10.50 cm, rods with average width of 600 nm and average length of 4.5 μm mixed with a small amount of microcubes (Figure 6b) were found in Sample 6. As farther from the furnace center, the $NiCl_2$ vapor concentration and the reaction temperature changed lower, which usually led to low concentrations of deposited product species and supplied the condition for the formation of 1D rods in Sample 6. Nevertheless, the thickness of the rods as large as 600 nm strongly indicates that the concentration of nickel species was still rather high and could even supply the formation of

SCHEME 2: Scheme of the Ni/SiO_2 Structure Formation Processes

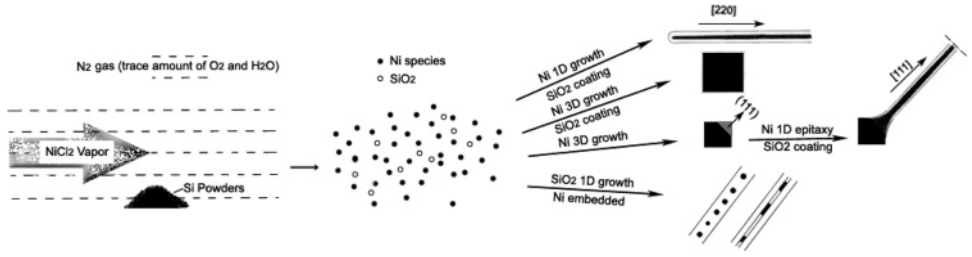

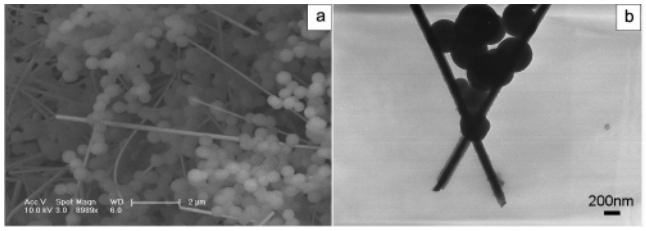

Figure 7. (a) SEM image of Sample 7. (b) TEM image of Sample 7.

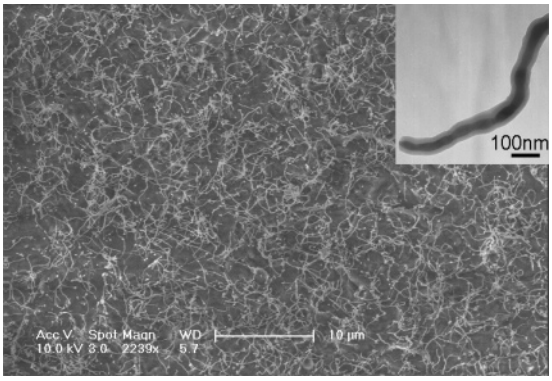

Figure 8. (a) SEM images of Sample 9 (inset: TEM image of Sample 9).

mirocubes due to fluctuations. Thus we can conclude that the supersaturation degree of the deposited species has played a very important role in determination of the product morphology.

The cube-tail structure should undergo first 3D growth and subsequent 1D epitaxy along the (111) direction, as has been determined in the preceding section. The assembly of nickel nanoparticles/nanorods occurs on the condition that SiO_2 reaches a relatively high concentration to support a spontaneous 1D growth. As a summary, an illustration of the formation process of the four types of Ni/SiO_2 structures is given in Scheme 2.

3.3 Synthesis of Silica-Sheathed Cobalt and Copper Particles. Furthermore, we tried to apply this method to Co and Cu, the neighboring elements of Ni, via the simple replacement of $NiCl_2$ by $CoCl_2$ or $CuCl_2$. Figure 7 and Figure S2 (in the Supporting Information) present a group of characterization results of Sample 7 (see Table 1 for the detailed experimental parameters). SEM (Figure 7a) and TEM (Figure 7b) images show that silica-sheathed nanoparticles with a diameter of 300−400 nm and nanowires with outer diameter of ∼100 nm and inner diameter of ∼80 nm were obtained. The XRD pattern (Figure S2a in the Supporting Information) demonstrates that the only crystal phase in the deposits is fcc cobalt (JCPDS, No. 15-0806). The EDS results (Figure S2b for the nanoparticles and Figure S2c for the nanowires in the Supporting Information) indicate that both of them consist of Co, Si, and O. With a variation of the experimental parameters as made for Sample 8, thick whiskers covered with a thin silica layer (see Figure S3, S4, and S5 in the Supporting Information) were formed.

Similarly, in the case of the copper element, curly sheathed nanowires were found in Sample 9 as shown in Figure 8. The existence of fcc Cu (JCPDS, No. 04-0836) and noncrystalline SiO_2 is confirmed by the XRD pattern (Figure S6a in the Supporting Information) and the EDS result (Figure S6b in the Supporting Information). The morphology could also change into other kinds such as Sample 10 (Figure S7, S8 and S9 in the Supporting Information) if the experimental parameters were properly changed. The above experimental data claim that this simple method has certain generality in the controlled synthesis of various silica-sheathed metal particles and is possibly applicable to other metals.

4. Conclusion

Various silica-sheathed nickel micro/nanostructures, from nanowires, microcubes, and nanocubes, with an epitaxial tail to 1D assembly structures of nanoparticles, have been prepared via a simple vapor−solid strategy. The growth and reaction mechanisms were investigated. Furthermore, the method proved to be successful for the shape-controlled synthesis of the neighboring elements of nickel in the periodic table (cobalt and copper) and is possibly effective to some other metals.

Acknowledgment. This work was supported by NSFC (50372030, 20130030), the Foundation for the Author of National Excellent Doctoral Dissertation of P. R. China, and the state key project of fundamental research for nanomaterials and nanostructures (2003CB716901). We thank Professor J. Acker, Department of Physical Chemistry, Freiberg University of Mining and Technology, Germany for the helpful discussions.

Supporting Information Available: Additional spectra and images of experimental samples. This material is available free of charge via the Internet at http://pubs.acs.org.

References and Notes

(1) Kroto, H. W.; Heath, J. R.; O'Brien, S. C.; Curl, R. F.; Smalley, R. E. *Nature* **1985**, *318*, 162.
(2) Iijima, S. *Nature* **1991**, *354*, 56.
(3) Alivisatos, A. P. *Science* **1996**, *271*, 933.
(4) Morales, A. M.; Lieber, C. M. *Science* **1998**, *279*, 208.
(5) Pan, Z. W.; Dai, Z. R.; Wang, Z. L. *Science* **2001**, *291*, 1947.
(6) Gudiksen, M. S.; Lauhon, L. J.; Wang, J.; Smith, D. C.; Lieber, C. M. *Nature* **2002**, *415*, 617.
(7) Xia, Y. N.; Rogers, J. A.; Paul, K. E.; Whitesides, G. M. *Chem. Rev.* **1999**, *99*, 1823.
(8) Wang, X.; Zhuang, J.; Peng, Q.; Li, Y. D. *Nature* **2005**, *437*, 122.
(9) Hu, J. Q.; Ma, X. L.; Shang, N. G.; Xie, Z. Y.; Wong, N. B.; Lee, C. S.; Lee, S. T. *J. Phys. Chem. B* **2002**, *106*, 3823.
(10) Yu, D. P.; Hang, Q. L.; Ding, Y.; Zhang, H. Z.; Bai, Z. G.; Wang, J. J.; Zou, Y. H.; Qian, W.; Xiong, G. C.; Feng, S. Q. *Appl. Phys. Lett.* **1998**, *73*, 3076.
(11) Raman, N. K.; Anderson, M. T.; Brinker, C. J. *Chem. Mater.* **1996**, *8*, 1682.
(12) Cassell, A. M.; Raymakers, J. A.; Kong, J.; Dai, H. J. *J. Phys. Chem. B* **1999**, *103*, 6484.
(13) Ma, R.; Bando, Y.; Sato, T. *Chem. Phys. Lett.* **2001**, *337*, 61.
(14) Hu, J. Q.; Bando, Y.; Zhan, J. H.; Golberg, D. *Angew. Chem., Int. Ed.* **2004**, *43*, 4606.
(15) Hu, J. Q.; Bando, Y.; Zhan, J. H.; Xu, F. F.; Sekiguchi, T.; Golberg, D. *Adv. Mater.* **2004**, *16*, 1465.
(16) Ge, J. P.; Li, Y. D. *Adv. Funct. Mater.* **2004**, *14*, 157.
(17) Ge, J. P.; Wang, J.; Zhang, H. X.; Li, Y. D. *Chem. Eur. J.* **2004**, *10*, 3525.
(18) Ge, J. P.; Wang, J.; Zhang, H. X.; Wang, X.; Peng, Q.; Li, Y. D. *Adv. Funct. Mater.* **2004**, *15*, 303.
(19) Zhang, H. X.; Ge, J. P.; Li, Y. D. *Chem. Vap. Deposition* **2005**, *11*, 147.
(20) Fu, Y. B.; Zhang, L. D. *J. Nanosci. Nanotechnol.* **2005**, *5*, 1113.
(21) Xu, D. X.; Das, S. R.; Peters, C. J.; Erickson, L. E. *Thin Solid Film* **1998**, *326*, 143.
(22) Jina, C. G.; Liu, W. F.; Jia, C.; Xiang, X. Q.; Cai, W. L.; Yao, L. Z.; Li, X. G. *J. Cryst. Growth* **2003**, *258*, 337.
(23) Binnewies, M.; Jug, K. *Eur. J. Inorg. Chem.* **2000**, *2000*, 1127.
(24) Lee, P. S.; Mangelinck, D.; Pey, K. L.; Ding, J.; Dai, J. Y.; Ho, C. S.; See, A. *Microelectron. Eng.* **2000**, *51*, 583.
(25) Zhang, H. X.; Ge, J. P.; Wang, J.; Wang, Z.; Yu, D. P.; Li, Y. D. *J. Phys. Chem. B* **2005**, *109*, 11585.